Ideal band shape in the potential thermoelectric material $CuAlO_2$: Comparison to Na_xCoO_2

Kouta Mori,[1,2] Hirofumi Sakakibara,[1] Hidetomo Usui,[1,2] and Kazuhiko Kuroki[2,3]
[1]*Department of Engineering Science, The University of Electro-Communications, Chofu, Tokyo 182-8585, Japan*
[2]*JST, ALCA, Gobancho, Chiyoda, Tokyo 102-0076, Japan*
[3]*Department of Physics, Osaka University, 1-1 Machikaneyama, Toyonaka, Osaka 560-0043, Japan*
(Received 7 March 2013; revised manuscript received 7 June 2013; published 26 August 2013)

A potential thermoelectric material $CuAlO_2$ is theoretically studied. We first construct a model Hamiltonian of $CuAlO_2$ based on the first principles band calculation, and calculate the Seebeck coefficient. Then, we compare the model with that of a well-known thermoelectric material Na_xCoO_2, and discuss the similarities and the differences. It is found that the two materials are similar from an electronic structure viewpoint in that they have a peculiar pudding-mold type band shape, which is advantageous for thermoelectric materials. There are, however, some differences, and we analyze the origin of the difference from a microscopic viewpoint. The band shape (a very flat band top but with an overall wide bandwidth) of $CuAlO_2$ is found to be even more ideal than that of Na_xCoO_2, and we predict that once a significant amount of holes is doped in $CuAlO_2$, thermoelectric properties (especially the power factor) even better than those of Na_xCoO_2 can be expected.

DOI: 10.1103/PhysRevB.88.075141 PACS number(s): 72.15.Jf, 71.20.−b

I. INTRODUCTION

The search for good thermoelectric materials serves as an intriguing challenge both from the viewpoint of fundamental physics as well as device applications.[1] Thermoelectric materials are often found in semiconductors, but the discovery of a large Seebeck coefficient found in Na_xCoO_2 (Ref. 2, Fig. 1 right panel), which exhibits a metallic nature of the conductivity opened up a new avenue for the search for thermoelectric materials. The coexistence of the large Seebeck coefficient S and the low resistivity ρ can give rise to a large power $P = S^2/\rho$, which is important from an application point of view. Soon after the discovery, the origin of the large thermopower in Na_xCoO_2 was studied theoretically, where the possible importance of the orbital degeneracy[3,4] or the narrow bandwidth[5] has been pointed out. Later on, one of the present authors, along with Arita, proposed that the peculiar band shape in which the top is flat but bends sharply into a dispersive portion plays an important role in the coexistence of the large Seebeck coefficient and the low resistivity in Na_xCoO_2.[6] This band has been referred to as the "pudding-mold" type. Recently, various materials with good thermoelectric properties, such as $CuRhO_2$,[7–9] Li_2RhO_4,[10,11] and $FeAs_2$,[12,13] have been shown to possess this type of band shape. The effect of the interplay between electron correlation and this kind of band shape has also been studied.[11,14–16]

Along this line of study, here we focus on $CuAlO_2$ (Fig. 1 left panel), which has also attracted much attention as a conducting transparent oxide,[17] and has motivated various theoretical studies.[18–20] In fact, several previous studies have pointed out a strong potential of this material as a good thermoelectric material,[21,22] although sufficient carrier doping to reduce the resistivity has not been successfully accomplished so far. In Refs. 21 and 23, a band structure calculation has been performed, which shows a flat portion at the top of the band, which is reminiscent of the band shape of Na_xCoO_2. In the present paper, we first construct a model Hamiltonian of $CuAlO_2$ based on the first principles band calculation, and calculate the Seebeck coefficient. We also consider the effect of bandwidth renormalization due to electron correlation effects that are not taken into account in the first principles band calculation.

Then, we compare the model with that of Na_xCoO_2, and discuss the similarities and the differences. We also analyze the origin of the difference of the band structure between the two materials from a microscopic point of view. The pudding-mold type band shape of $CuAlO_2$ is found to be even more ideal than that of Na_xCoO_2, and we predict that once a significant amount of holes is doped in $CuAlO_2$, thermoelectric properties (especially the power factor) even better than those of Na_xCoO_2 can be expected. This is due to the combination of an extremely ideal band shape (that enhances the Seebeck coefficient) and a relatively wide bandwidth (that can give large conductivity when the holes are doped).

II. CONSTRUCTION OF THE SINGLE ORBITAL MODEL

We perform a first principles band calculation of $CuAlO_2$ using the WIEN2K package.[24] We adopt the lattice structure parameters given in Ref. 23. Here we take $RK_{\max} = 7{,}512$ k points, and adopt the Perdew-Burke-Ernzerhof generalized gradient approximation (PBE-GGA) exchange correlation functional.[25] The calculation result is shown as dashed lines in Fig. 2, which is essentially the same as those obtained in previous studies.[21,23] Namely, there is a flat portion around the Brillouin zone edge, which bends sharply into a dispersive portion as the Γ point is approached. This is nothing but the pudding-mold type band introduced in Ref. 6.

Since the flat portion of the band is well isolated from other portions, we can extract this portion and construct a single orbital model, where we exploit the maximally localized Wannier orbitals.[26,27] Here, the extracted orbital is obtained by projecting onto the $3d_{3z^2-r^2}$ orbital, namely, the obtained Wannier orbital has a strong Cu $3d_{3z^2-r^2}$ character, while the contributions from other orbitals due to the hybridization are implicitly taken into account in this single Wannier orbital. The result is shown in Fig. 2 as a solid line superposed to the first principles result.

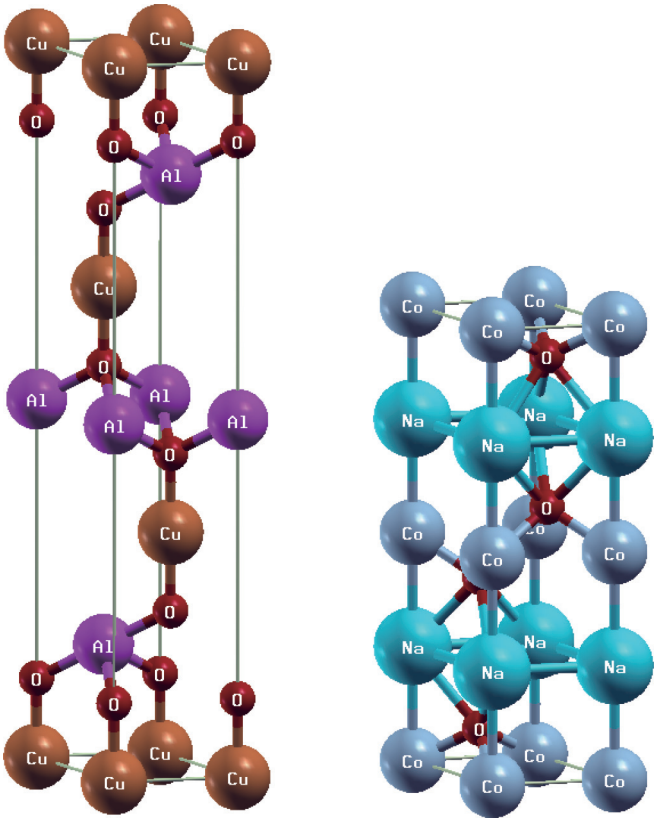

FIG. 1. (Color online) The lattice structure of $CuAlO_2$ (left) and Na_xCoO_2 (right).

III. SEEBECK COEFFICIENT AND POWER FACTOR

A. The Boltzmann's equation approach

In this section we calculate the Seebeck coefficient adopting the single orbital model and using the Boltzmann's equation approach, In this approach, tensors of the Seebeck coefficient $\boldsymbol{S}$ and the conductivity $\boldsymbol{\sigma}$ are given as

$$\boldsymbol{S} = \frac{1}{eT}\boldsymbol{K}_1\boldsymbol{K}_0^{-1}, \tag{1}$$

$$\boldsymbol{\sigma} = e^2\boldsymbol{K}_0, \tag{2}$$

where e (<0) is the elementary charge, T is the temperature, tensors $\boldsymbol{K}_1$,$\boldsymbol{K}_2$ are given as

$$\boldsymbol{K}_n = \sum_{\boldsymbol{k}} \tau(\boldsymbol{k})\boldsymbol{v}(\boldsymbol{k})\boldsymbol{v}(\boldsymbol{k})\left[-\frac{df(\epsilon)}{d\epsilon}(\boldsymbol{k})\right][\epsilon(\boldsymbol{k})-\mu]^n . \tag{3}$$

Here, $\epsilon(\boldsymbol{k})$ is the band dispersion, $\boldsymbol{v}(\boldsymbol{k}) = \frac{1}{\hbar}\nabla_{\boldsymbol{k}}\epsilon(\boldsymbol{k})$ is the group velocity, $\tau(\boldsymbol{k})$ is the quasiparticle lifetime, $f(\epsilon)$ is the Fermi distribution function, and μ is the Fermi level (chemical potential). Here, due to the derivative of the Fermi distribution function $df(\epsilon)/d\epsilon$, large contributions to K_0 and K_1 come from within k_BT from the Fermi level μ. In the present study, we approximate τ as a constant, so that it cancels out in the Seebeck coefficient. We simply write σ_{xx} and S_{xx} as σ and S, respectively. σ and thus the power factor σS^2 contain the constant τ, whose absolute value is not determined. Therefore, we only discuss the values of the power factor normalized by its maximum value as a function of hole doping rate. We note here that the constant τ approximation was also adopted in the study of Na_xCoO_2 in Ref. 6, which gave very good agreement with the experiments as far as the bandwidth renormalization was taken into account. Since the origin of the pudding-mold type band is essentially the same between Na_xCo_2 and $CuAlO_2$ (both originating from a $3d_{3z^2-r^2}$-like orbital of a transition metal), we continue to use this approximation in the present study, while we investigate the bandwidth renormalization effect due to electron correlation in Sec. IV.

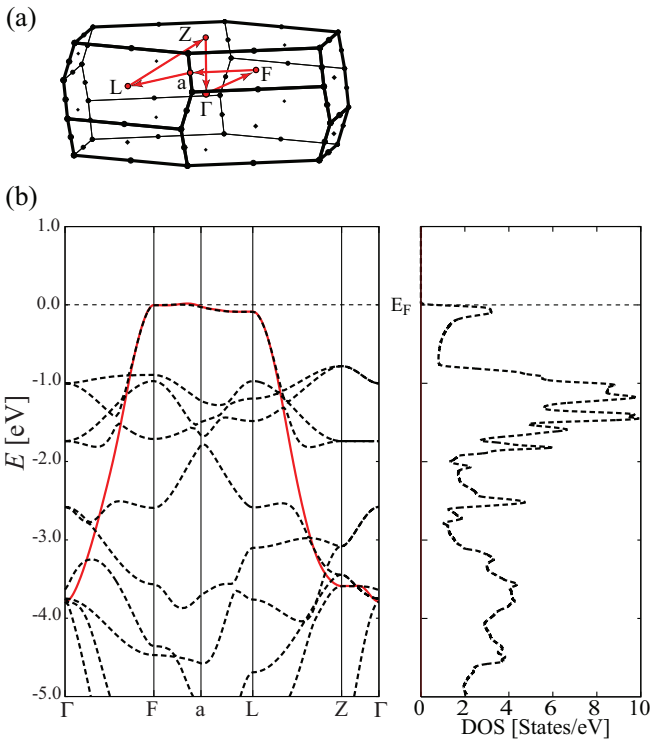

FIG. 2. (Color online) (a) The Brillouin zone. (b) Left: The first principles band calculation result of $CuAlO_2$ (dashed lines) and the single orbital model (solid line). Right: The density of states.

B. The pudding-mold type band

As discussed in Ref. 6, the pudding-mold type band is advantageous in obtaining a large Seebeck coefficient despite low resistivity. For a constant τ, Eq. (3) can roughly be approximated as

$$\begin{aligned} K_0 &= \tau\sum_k \left(v_{\text{above}}^2 + v_{\text{below}}^2\right), \\ K_1 &= \tau\sum_k \left(v_{\text{above}}^2 - v_{\text{below}}^2\right), \end{aligned} \tag{4}$$

where v_{above} and v_{below} are group velocities above and below the Fermi level (representative values within k_BT from the Fermi level). Since the Seebeck coefficient is proportional to K_1/K_0, a larger difference between v_{above} and v_{below} gives larger S. Physically, this means that a large difference in the group velocities of holes and electrons results in a large Seebeck coefficient. When the Fermi level lies near the band edge, this difference (the $v_{\text{below}}/v_{\text{above}}$ ratio) can be large but the absolute values of the velocities are small, so that the conductivity becomes small. On the other hand, in usual metallic systems, in which the Fermi level lies in the middle

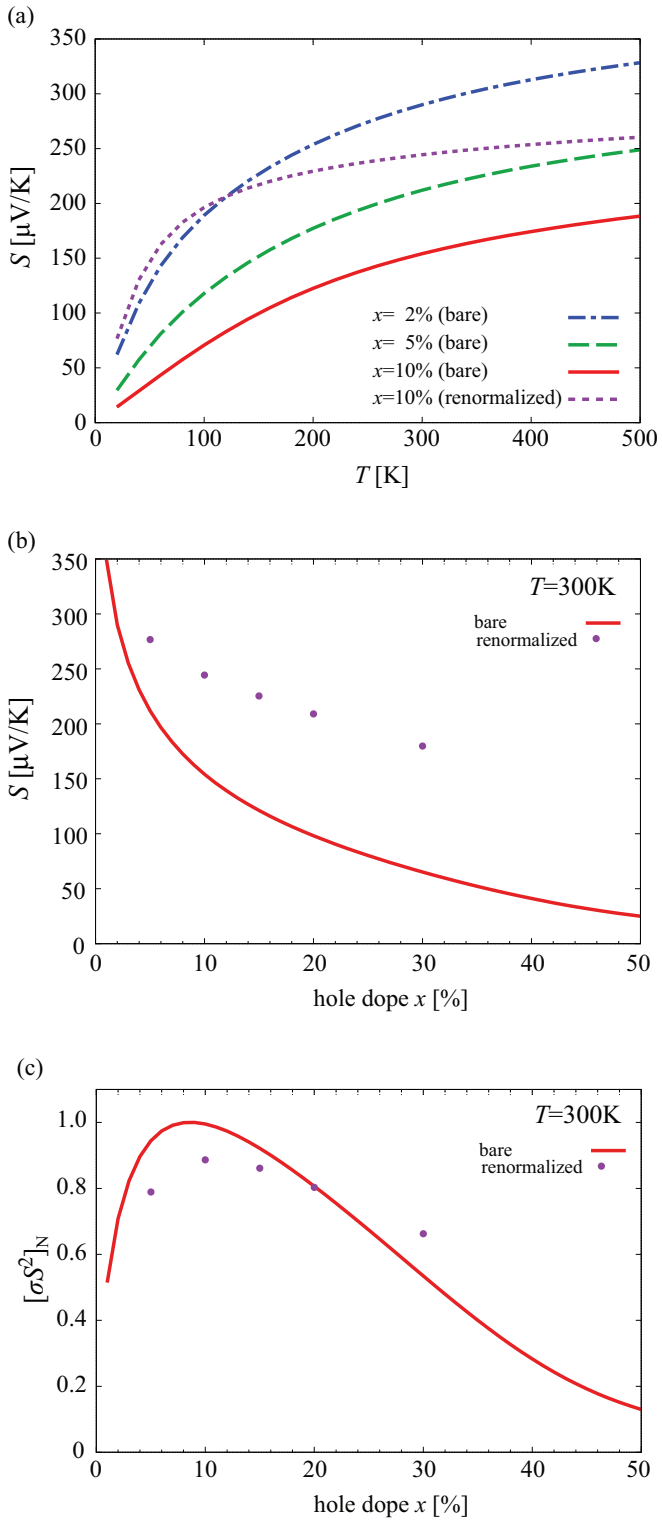

FIG. 3. (Color online) The calculated thermoelectric properties of $CuAlO_2$. (a) The Seebeck coefficient against temperature for 2% (dashed-dotted), 5% (long dashed), and 10% (solid) hole doping obtained using the bare band structure, and for 10% doping using the renormalized band (dashed). (b) The Seebeck coefficient against the hole doping concentration at $T = 300$ K obtained using the bare (solid line) and the renormalized bands (dots). (c) The normalized power factor against the doping concentration at $T = 300$ K obtained for the bare (solid) and the renormalized bands (dots). See Sec. IV for the calculation result using the renormalized band structure.

of the bands where v_{above} and v_{below} have similar values, the Seebeck coefficient tends to be small. This is the reason why a large power factor σS^2 is usually difficult to obtain. For the pudding-mold type band, however, the large density of states at the top of the band prevents the Fermi level from going down rapidly even when a large amount of carriers (holes in the present case) is doped, and when the Fermi level sits close to the bending point of the band, K_1 is large because of the small v_{above} due to the flat portion and the large v_{below} due to the dispersive portion of the band. In this manner, the coexistence of a large Seebeck coefficient and small resistivity is realized for a wide range of hole doping ratios.

C. Calculation results

Figure 3 shows the Seebeck coefficient calculated for the single orbital model of $CuAlO_2$. Figure 3(a) shows the temperature dependence for 2%, 5%, and 10% hole doping, and Fig. 3(b) is the doping dependence at $T = 300$ K. These calculated values [e.g., ∼210 (150) μV/K at $T = 300$ K for 5% (10)% doping] are similar but somewhat smaller compared to those values calculated for the single band model of Na_xCoO_2 in Ref. 6. It should be noted that in Ref. 6, the bandwidth was reduced "by hand" from its original first principles calculation value of $\simeq$2 down to $\simeq$1 eV so as to fit the angle resolved photoemission data, thereby taking into account the bandwidth renormalization effect. In the present calculation result of Fig. 3, the original first principles band structure is adopted, whose width is about 4 eV, i.e., four times wider than that for Na_xCoO_2 in Ref. 6. Therefore, a more direct comparison should be made after the bandwidth renormalization is taken into account, which will be done in Sec. IV.

The maximum power factor is reached at around 10% hole doping, which is a rather large doping rate, and is in fact similar to the situation in Na_xCoO_2.[6] This is another feature peculiar to the pudding-mold type band, where a large amount of doping does not result in a rapid reduction of the Fermi level. It should be noted that ∼10% doping gives the maximum power factor within the constant lifetime (τ) approximation. In reality, the lifetime may decrease as the doping ratio is increased, so that the maximum power factor is reached for a smaller doping.

IV. EFFECT OF THE BANDWIDTH RENORMALIZATION

A. Self-energy correction

In this section, we study the effect of the bandwidth renormalization due to the many-body correlation. We consider a many-body Hamiltonian that considers the on-site repulsive interaction in the single band model. We obtain the self-energy correction due to the many-body interaction within the fluctuation exchange (FLEX) approximation,[28] thereby taking into account the effect of spin and charge fluctuations that were omitted in the first principles calculation. In FLEX, the Green's function $G(\mathbf{k}, i\omega_n)$ is calculated by solving the Dyson equation. The self-energy $\Sigma(\mathbf{k}, i\omega_n)$ in the Dyson equation is calculated by summing up bubble and ladder diagrams constructed from the Green's function that is determined self-consistently. This calculation is performed by taking $32 \times 32 \times 32$ k-point meshes and 4096 Matsubara frequencies with the temperature $T = 0.01$ eV. The quasiparticle excitation dispersion can be

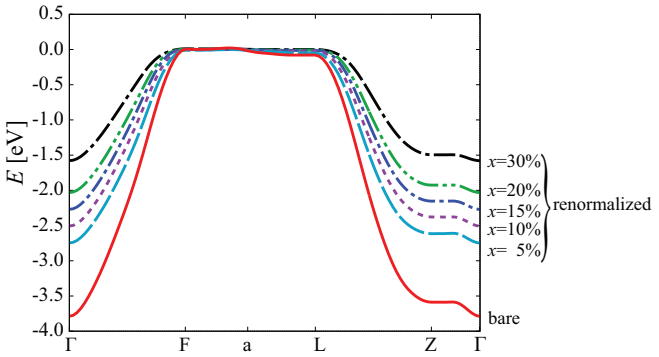

FIG. 4. (Color online) The renormalized band dispersion obtained for various doping ratios for $U = 2.5$ eV. The red solid line is the bare band dispersion.

obtained by

$$\omega(\mathbf{k}) = z_{\vec{k}}^{-1}\{\varepsilon(\mathbf{k}) - \mu + \mathrm{Re}\,\Sigma^R(\mathbf{k},\omega = 0)\}, \tag{5}$$

where $\varepsilon(\mathbf{k})$ is the bare band dispersion and Σ^R is the retarded self-energy, which is approximated as $\mathrm{Re}\,\Sigma^R(\mathbf{k},\omega = 0) \simeq \mathrm{Re}\,\Sigma(\mathbf{k},i\pi k_B T)$ taking the lowest Matsubara frequency. The mass enhancement factor is obtained as

$$z_{\mathbf{k}} = 1 - \left.\frac{\partial \Sigma^R(\mathbf{k},\omega)}{\partial \omega}\right|_{\omega\to 0} \simeq 1 - \frac{\mathrm{Im}\,\Sigma(\mathbf{k},i\pi k_B T)}{\pi k_B T}. \tag{6}$$

In Fig. 4, we show the renormalized band dispersion for several hole doping ratios obtained for a typical on-site repulsion of 2.5 eV. It can be seen that the bandwidth is monotonically renormalized as the holes are doped.

B. Seebeck coefficient and power factor

Here we calculate the Seebeck effect using the renormalized band and adopting the Boltzmann's equation approach described in Sec. III A. The results are given in Fig. 3 with circles. The temperature dependence of the Seebeck coefficient shows that it is strongly enhanced, especially at low temperatures, compared to that calculated using the original band structure. Also, the doping dependence of the Seebeck coefficient at 300 K shows that large values are maintained up to large doping concentrations. The doping dependence of the power factor is normalized by the maximum value for the original band structure. The result at 300 K shows that the maximum value takes roughly a similar value as in the original case, while the doping dependence becomes less prominent. The power factor, as a whole, is not enhanced by electron correlation despite the strong enhancement in the Seebeck coefficient because the conductivity is suppressed due to the reduction of the group velocity.

Let us now make a somewhat quantitative comparison with the single band model of Na_xCoO_2 in Ref. 6, where the bandwidth renormalization effect was taken into account by fitting the angle resolved photoemission data. From the doping dependence of the Seebeck coefficient at 300 K in Fig. 3, it can be seen that the obtained values ~280 and ~250 μV/K at 5% and 10% doping, respectively, are larger compared to the corresponding values 250 and 200 μV/K for the single band model of Na_xCoO_2.[6] This occurs despite the renormalized bandwidth being wider (>2 eV for <10% doping) in the present case than that in Na_xCoO_2 (~1 eV). Since a wider bandwidth (a larger group velocity in the dispersive portion of the band) is favorable for obtaining large conductivity, the present result suggests that the band *shape* of $CuAlO_2$ (an extremely flat band top bending sharply into a dispersive portion) is even more ideal than that of Na_xCoO_2 from the viewpoint of the power factor.

V. ORIGIN OF THE PUDDING-MOLD TYPE BAND

A. The effect of the second- and third-nearest-neighbor hoppings

Both $CuAlO_2$ and Na_xCoO_2 exhibit a pudding-mold type band. Here we discuss its origin from the viewpoint of the hopping integrals on the triangular lattice. Here we focus on the band structure within the planes, and neglect the hopping integral in the z direction. The renormalization due to electron correlation will not be considered here. In Fig. 5, we show the band structure of the single band model of both materials in the Brillouin zone of the two-dimensional triangular lattice, in which the hoppings up to fifth nearest neighbors are extracted (t_1–t_5, the original model contains

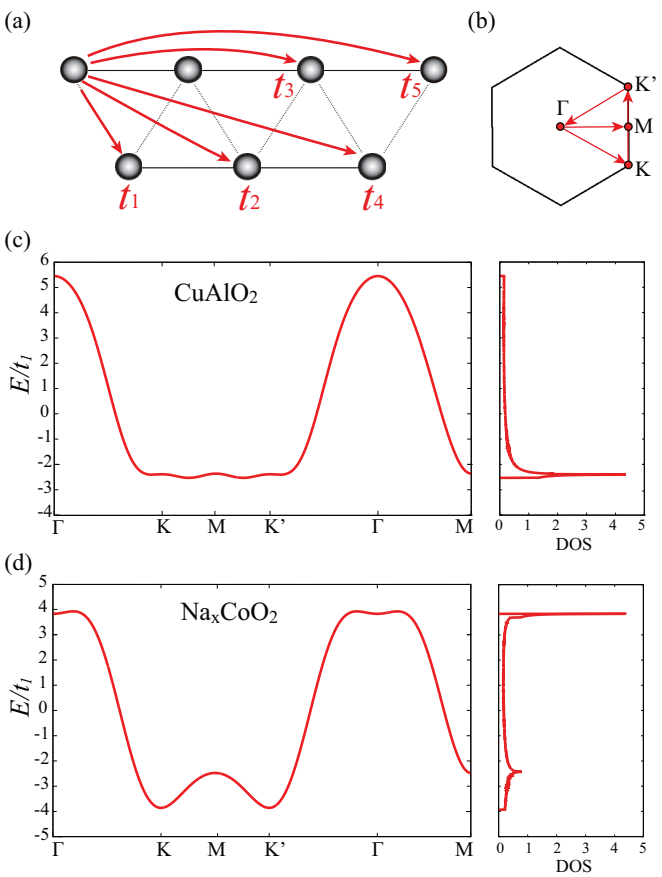

FIG. 5. (Color online) (a) The definition of the hoppings on the triangular lattice. (b) The two-dimensional Brillouin zone. (c), (d) Band dispersion normalized by t_1 and the density of states of the two-dimensional models of $CuAlO_2$ and Na_xCoO_2 which considers the extracted hoppings t_1–t_5.

TABLE I. The hoppings for the single orbital model of $CuAlO_2$ and Na_xCoO_2.

	t_1 (eV)	t_2/t_1	t_3/t_1	t_4/t_1	t_5/t_1
$CuAlO_2$	−0.45	0.003	−0.069	−0.030	0.034
Na_xCoO_2	0.18	−0.24	−0.15	−0.001	0.008

very small hoppings between more distant sites). The band structure is normalized by the nearest-neighbor hopping t_1. Note that the band structure of $CuAlO_2$ is turned upside down compared to the original one because $t_1 < 0$. The hoppings normalized by t_1 are given in Table I. From this comparison, it can be seen that the flat portion of the band occurs around the Brillouin zone edge in $CuAlO_2$, while the flat portion of the band structure of Na_xCoO_2 is around the Γ point. Note that the path along the Brillouin zone edge *K*-*M* in the two-dimensional Brillouin zone corresponds to lines such as *a*-*L* (or *F*) in the three-dimensional Brillouin zone shown in Fig. 2(a).

To see the origin of this difference between the two materials, we vary the hopping integrals t_2 and t_3 "by hand." As shown in Fig. 6, the second-nearest-neighbor hopping has a dramatic effect of making the band around the Γ point flat while making it around *K*-*M* dispersive. Consequently, the peak structure of the density of states moves largely from $E < 0$ to $E > 0$ as the absolute value of $t_2 < 0$ is increased. The third-nearest-neighbor hopping $t_3 < 0$, on the other hand, has the effect of reversing the dispersion around *K*-*M*, so that the band around *K*-*M* once becomes nearly perfectly flat (around $t_3/t_1 = -0.1$) as $|t_3|$ is increased.

Now, if we go back to the hopping integrals of the two materials given in Table I, there is a large difference, i.e., $|t_2/t_1|$ is almost negligible in $CuAlO_2$ compared to that in Na_xCoO_2. This, along with t_3/t_1 being somewhat close to −0.1, makes the band around *K*-*M* fairly flat in $CuAlO_2$. Strictly speaking, $t_3/t_1 \sim -0.07$ is still somewhat away from $t_3/t_1 = -0.1$, where a nearly perfectly flat band appears. Actually, we find that there is also the effect of $t_5/t_1 > 0$, which makes the band around *K*-*M* flat, while enhancing the dispersion around the Γ point. In sharp contrast to $CuAlO_2$, the combined effect of t_2 and t_3 in Na_xCoO_2 makes the band around the Γ point flat, while enhancing the dispersion around the Brillouin zone edge *K*-*M*.

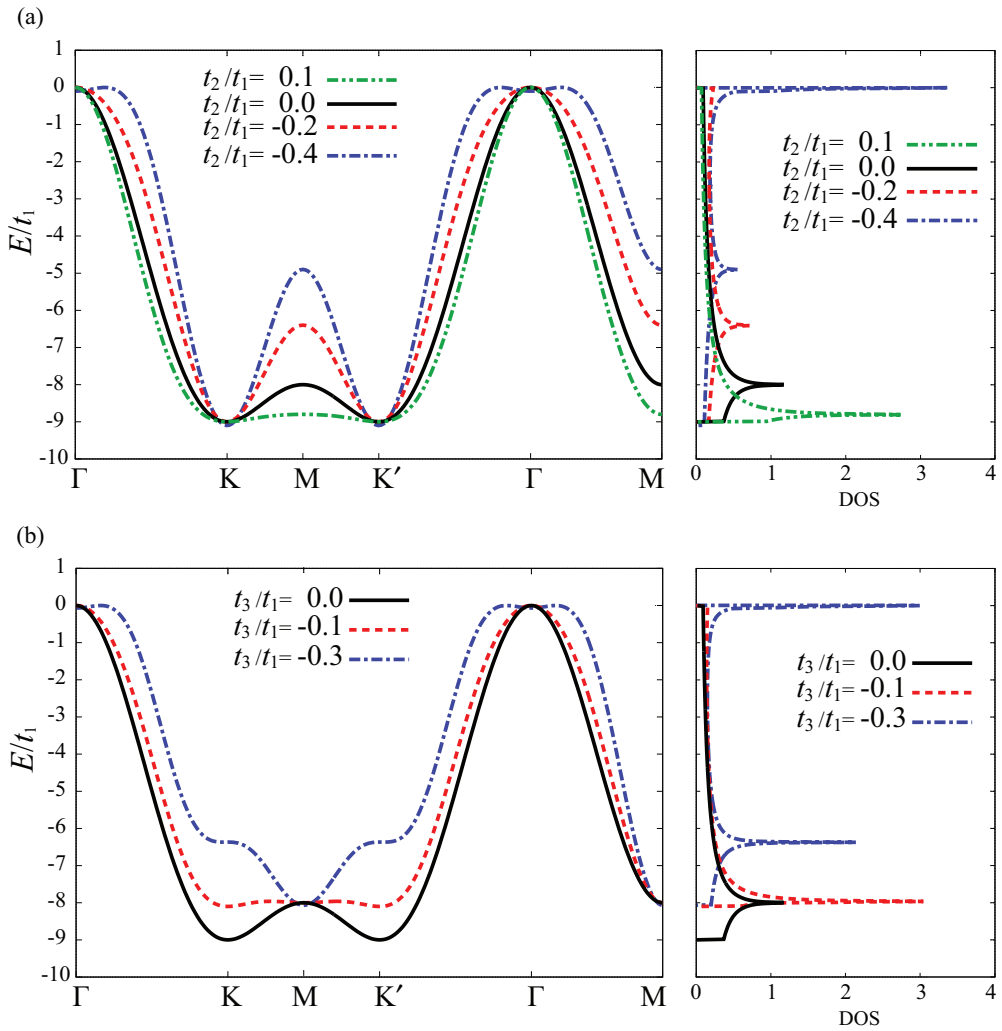

FIG. 6. (Color online) Band dispersion of the single orbital model on the triangular lattice in which only (a) t_1 and t_2 or (b) t_3 are considered.

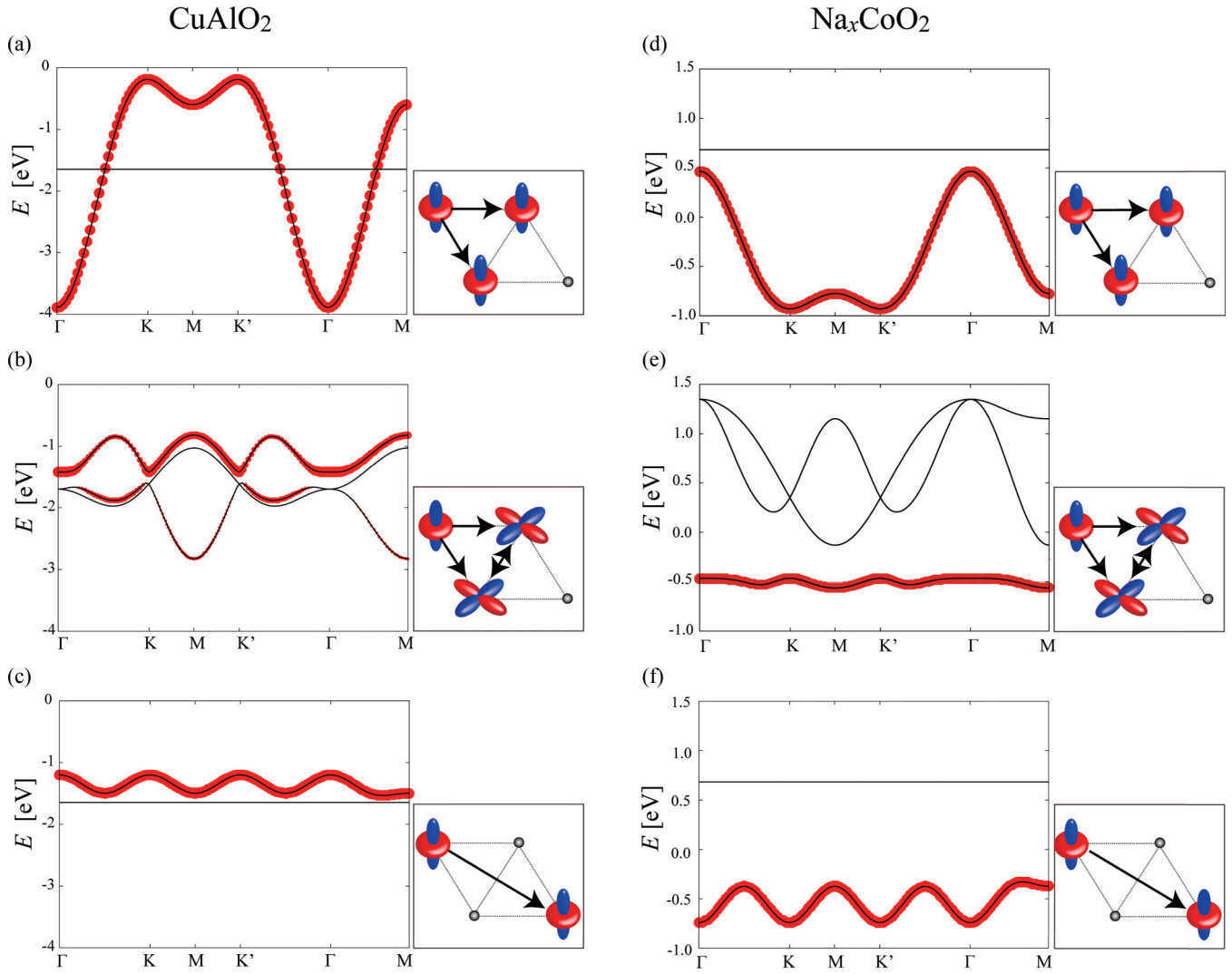

FIG. 7. (Color online) Band dispersion of models constructed by extracting some of the orbitals and hoppings from the 3*d* five orbital models of $CuAlO_2$ [(a)–(c)] and Na_xCoO_2 [(d), (e)]. The thickness of the lines represents the strength of the $d_{3z^2-r^2}$ orbital character. (a), (d) Only the $d_{3z^2-r^2}$ orbital is extracted, and only the nearest-neighbor hopping is considered. (b), (e) $d_{3z^2-r^2}$ and d_{xy/x^2-y^2} orbitals are extracted, and only the nearest-neighbor interorbital hopping is considered. (c), (f) Only the $d_{3z^2-r^2}$ orbital is extracted, and only the second-nearest-neighbor hopping is considered.

B. The origin of the difference between $CuAlO_2$ and Na_xCoO_2

In this section, we discuss the origin of the difference in the second neighbor hopping between $CuAlO_2$ and Na_xCoO_2. To see this, we now construct models of these materials where all of the five 3*d* orbitals are considered explicitly. Here, the difference between the $d_{3z^2-r^2}$ orbital in the five orbital model and the $d_{3z^2-r^2}$ orbital mentioned in the previous sections should be noted. The $d_{3z^2-r^2}$ Wannier orbital in the previous sections consists not only of the $d_{3z^2-r^2}$ in the five orbital sense, but also of the other hybridized orbitals as well. In other words, the $d_{3z^2-r^2}$ Wannier orbital of the single orbital model considered in the previous sections takes into account the effect of other orbitals implicitly. Since the band structure in the vicinity of the Fermi level is the same between the single and the five orbital models, the two models give the same transport properties.

In the five orbital model, the most relevant band originates from the $d_{3z^2-r^2}$ orbital[29] in both $CuAlO_2$ and Na_xCoO_2, but other orbitals can make a contribution to the band shape due to the hybridization. To see this effect, we first hypothetically vary the on-site energy of the orbitals other than $d_{3z^2-r^2}$. We find that the $d_{xz/yz}$ orbitals have a small effect on the band shape in both of the materials. On the other hand, we find that varying the on-site energy of the d_{xy/x^2-y^2} orbitals affects the flatness of the band top only in $CuAlO_2$. This means that there is a hybridization between $d_{3z^2-r^2}$ and d_{xy/x^2-y^2} orbitals which plays an important role in producing the pudding-mold type band in $CuAlO_2$.

To further investigate this point, we consider the effects of the intraorbital and interorbital hoppings step by step. In Figs. 7(a) and 7(c), we show the band dispersion in which only the $d_{3z^2-r^2}$ orbital is extracted from the five 3*d* orbitals, and only the nearest-neighbor [Fig. 7(a)] or the second-nearest-neighbor hopping [Fig. 7(c)] is considered. In the band dispersion shown in Fig. 7(b), we extract three orbitals out of five, namely, $d_{3z^2-r^2}$ and d_{xy/x^2-y^2}, and consider only the nearest-neighbor interorbital hoppings between the

$d_{3z^2-r^2}$ and d_{xy/x^2-y^2} orbitals. Here, the thickness of the lines represents the magnitude of the $d_{3z^2-r^2}$ orbital weight. This result shows that the effect of the interorbital $d_{3z^2-r^2}$-d_{xy/x^2-y^2} orbital hopping pushes up the $d_{3z^2-r^2}$ band top around the M point. This effect is taken into account as a positive contribution to t_2/t_1 in the single orbital model which considers the effect of d_{xy/x^2-y^2} implicitly. Namely, the hopping path $d_{3z^2-r^2} \rightarrow d_{xy/x^2-y^2} \rightarrow d_{3z^2-r^2}$ gives a positive contribution to the effective t_2/t_1 between second neighbor $d_{3z^2-r^2}$ orbitals. On the other hand, there is a negative contribution to t_2/t_1 of the single orbital model coming from the direct second-nearest-neighbor $d_{3z^2-r^2}$-$d_{3z^2-r^2}$ hopping in the five orbital model, which pushes down the band around the M point, as shown in Fig. 7(c). In $CuAlO_2$, the positive and negative contributions almost cancel each other out, resulting in a very small t_2/t_1 in the single orbital model.

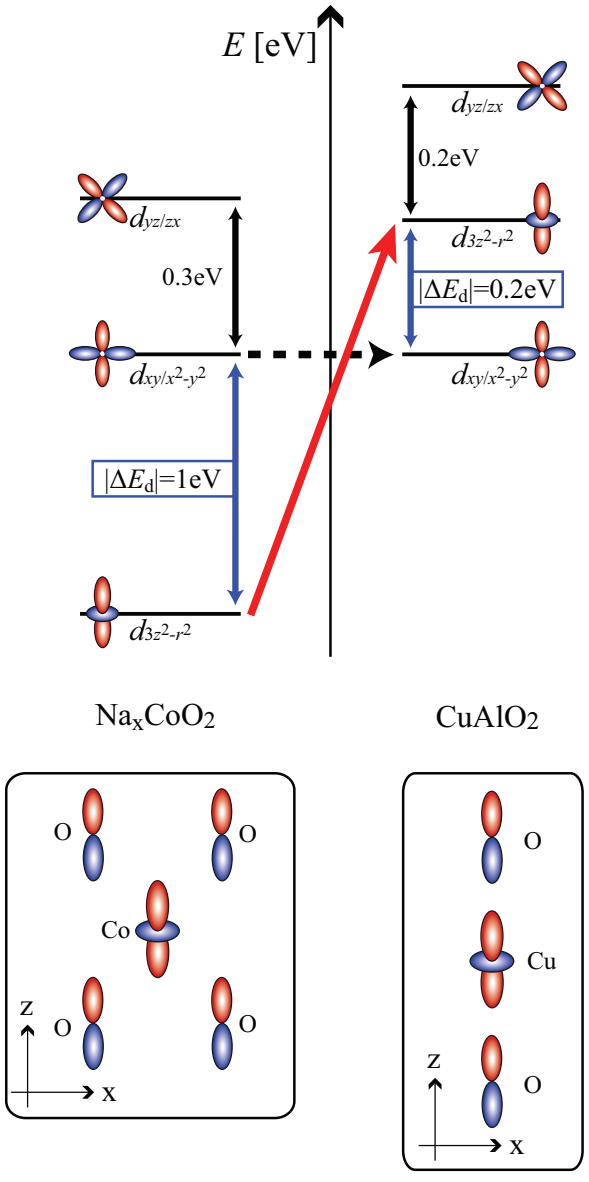

FIG. 8. (Color online) The energy levels of the five orbital model of Na_xCoO_2 (left) and $CuAlO_2$ (right). The bottom figure shows the difference in the ligand position between the two materials.

A similar five orbital analysis for Na_xCoO_2, shown in Figs. 7(d)–7(f), reveals that the situation is different. From Fig. 7(e), it can be seen that the dispersion originating from the $d_{3z^2-r^2}$-d_{xy/x^2-y^2} hybridization is very small, namely, the contribution of the $d_{3z^2-r^2} \rightarrow d_{xy/x^2-y^2} \rightarrow d_{3z^2-r^2}$ path to t_2 in the single orbital model is negligible. On the other hand, there is a direct $d_{3z^2-r^2}$-$d_{3z^2-r^2}$ second neighbor hopping, which gives a positive contribution to t_2/t_1 in the single orbital model, pushing up the band around the M point. Hence, in Na_xCoO_2, t_2/t_1 is large and the flatness of the band does not appear around K-M-K.

The origin of the difference between the two materials in the contribution of the $d_{3z^2-r^2} \rightarrow d_{xy/x^2-y^2} \rightarrow d_{3z^2-r^2}$ path comes from the difference in the energy level offset between $d_{3z^2-r^2}$ and d_{xy/x^2-y^2} in the five orbital model $\Delta E_d = E(d_{xy/x^2-y^2}) - E(d_{3z^2-r^2})$. As shown in Fig. 8, this offset is large in Na_xCoO_2, while relatively small in $CuAlO_2$. A smaller energy difference gives a larger contribution of the $d_{3z^2-r^2} \rightarrow d_{xy/x^2-y^2} \rightarrow d_{3z^2-r^2}$ path. The difference in ΔE_d can be understood from the lattice structure. As shown in the bottom of Fig. 8, the oxygen atoms in $CuAlO_2$ are located at positions toward which the $d_{3z^2-r^2}$ orbitals are elongated, while that is not the case for Na_xCoO_2. Therefore, the crystal field of the ligand atoms pushes up the $d_{3z^2-r^2}$ level, locating it just above the d_{xy/x^2-y^2} level.

VI. CONCLUSION

To conclude, $CuAlO_2$ is a very good candidate for a thermoelectric material with a large Seebeck coefficient coexisting with large conductivity. The origin of this is the pudding-mold band similar to, but different from, the one in Na_xCoO_2. In $CuAlO_2$, the negligibly small second-nearest-neighbor hopping does not affect the flat portion of the band around the Brillouin zone edge already present in the nearest-neighbor hopping model on the triangular lattice. Moreover, the additional presence of the third (and the fifth) hopping integrals makes the band even more flat around the Brillouin zone edge. This is in sharp contrast with the case of Na_xCoO_2, where the large second-nearest-neighbor hopping moves the flat portion of the band to the Γ point area. The difference in the band shape between the two materials comes from the difference in the electron hopping between the second neighbor $d_{3z^2-r^2}$ orbital mediated by d_{xy/x^2-y^2} in the five orbital sense. Namely, in $CuAlO_2$, the $d_{3z^2-r^2}$ and d_{xy/x^2-y^2} energy levels are close to each other, giving rise to a large contribution from the path $d_{3z^2-r^2} \rightarrow d_{xy/x^2-y^2} \rightarrow d_{3z^2-r^2}$, which nearly cancels out the direct $d_{3z^2-r^2}$-$d_{3z^2-r^2}$ contribution to the second neighbor hopping. The difference in the energy difference between $d_{3z^2-r^2}$ and d_{xy/x^2-y^2} levels comes from the position of the oxygen atoms. A large Seebeck coefficient comparable to the model of Na_xCoO_2, despite a wider bandwidth, implies that the band shape is extremely ideal, and very good thermoelectric properties, especially a large power factor, are expected once a large amount of hole doping is accomplished.

ACKNOWLEDGMENT

We would like to thank M. Nohara for fruitful discussions. Part of the calculation has been done on the computer facilities, ISSP, University of Tokyo. H.S. acknowledges support from JSPS (Grant No. 23009446).

[1]For a general review on the theoretical aspects as well as experimental observations of thermopower, see G. D. Mahan, Solid State Phys. **51**, 81 (1997).
[2]I. Terasaki, Y. Sasago, and K. Uchinokura, Phys. Rev. B **56**, R12685 (1997).
[3]W. Koshibae, K. Tsutsui, and S. Maekawa, Phys. Rev. B **62**, 6869 (2000).
[4]W. Koshibae and S. Maekawa, Phys. Rev. Lett. **87**, 236603 (2001).
[5]D. J. Singh, Phys. Rev. B **61**, 13397 (2000).
[6]K. Kuroki and R. Arita, J. Phys. Soc. Jpn. **76**, 083707 (2007).
[7]H. Kuriyama, M. Nohara, T. Sasagawa, K. Takubo, T. Mizokawa, K. Kimura, and H. Takagi, *Proceedings of the 25th International Conference on Thermoelectrics* (IEEE, Piscataway, NJ, 2006).
[8]S. Shibasaki, W. Kobayashi, and I. Terasaki, Phys. Rev. B **74**, 235110 (2006).
[9]H. Usui, R. Arita, and K. Kuroki, J. Phys.: Condens. Matter **21**, 064223 (2009).
[10]Y. Okamoto, S. Niitaka, M. Uchida, T. Waki, M. Takigawa, Y. Nakatsu, A. Sekiyama, S. Suga, R. Arita, and H. Takagi, Phys. Rev. Lett. **101**, 086404 (2008).
[11]R. Arita, K. Kuroki, K. Held, A. V. Lukoyanov, S. Skornyakov, and V. I. Anisimov, Phys. Rev. B **78**, 115121 (2008).
[12]P. Sun, N. Oeschler, S. Johnsen, B. B. Iversen, and F. Steglich, Appl. Phys. Express **2**, 091102 (2009).
[13]H. Usui, K. Kuroki, S. Nakano, K. Kudo, and M. Nohara, arXiv:1211.7176.
[14]P. Wissgott, A. Toschi, H. Usui, K. Kuroki, and K. Held, Phys. Rev. B **82**, 201106 (2010).
[15]P. Wissgott, A. Toschi, G. Sangiovanni, and K. Held, Phys. Rev. B **84**, 085129 (2011).
[16]H. Usui, Ph.D. thesis, University of Electro-Communications, Tokyo, 2012.
[17]H. Kawazoe, M. Yasukawa, H. Hyodo, M. Kurita, H. Yanagi, and H. Hosono, Nature (London) **389**, 939 (1997).
[18]Q.-J. Liu, Z.-T. Liu, L.-P. Feng, H. Tan, W.-T. Liu, and F. Yan, Appl. Phys. Lett. **97**, 141917 (2010).
[19]C. K. Ghosh, D. Sarkar, M. K. Mitra, and K. K. Chattopadhyay, J. Phys.: Condens. Matter **24**, 235501 (2012).
[20]J. Vidal, F. Trani, F. Bruneval, M. A. L. Marques, and S. Botti, Phys. Rev. Lett. **104**, 136401 (2010).
[21]H. Katayama-Yoshida, T. Koyanagi, H. Funashima, H. Harima, and A. Yanase, Solid State Commun. **126**, 135 (2003).
[22]P. Poopanya, A. Yangthaisong, C. Rattanapun, and A. Wichainchai, J. Electron. Mater. **40**, 987 (2011).
[23]A. Nakanishi and H. Katayama-Yoshida, Solid State Commun. **152**, 24 (2012).
[24]P. Blaha, K. Schwarz, G. K. H. Madsen, D. Kvasnicka, and J. Luitz, *Wien2k: An Augmented Plane Wave + Local Orbitals Program for Calculating Crystal Properties* (Vienna University of Technology, Wien, 2001).
[25]J. P. Perdew, K. Burke, and M. Ernzerhof, Phys. Rev. Lett. **77**, 3865 (1996).
[26]N. Marzari and D. Vanderbilt, Phys. Rev. B **56**, 12847 (1997); I. Souza, N. Marzari, and D. Vanderbilt, *ibid.* **65**, 035109 (2001); the Wannier functions are generated by the code developed by A. A. Mostofi, J. R. Yates, N. Marzari, I. Souza, and D. Vanderbilt, http://www.wannier.org/
[27]J. Kunes, R. Arita, P. Wissgott, A. Toschi, H. Ikeda, and K. Held, Comput. Phys. Commun. **181**, 1888 (2010).
[28]N. E. Bickers, D. J. Scalapino, and S. R. White, Phys. Rev. Lett. **62**, 961 (1989).
[29]For Na_xCoO_2, the following notation is more commonly used (Ref. 5). The $3d$ orbitals consist of the low-lying t_{2g} and the high-lying e_g orbitals, and the t_{2g} orbitals are split into a_{1g} and e'_g orbitals. In the present notation, the $d_{3z^2-r^2}$ orbital corresponds to the commonly used a_{1g} orbital. We will call this the "$d_{3z^2-r^2}$ orbital" in the sense that it is the maximally localized Wannier orbital obtained by projecting onto the $d_{3z^2-r^2}$ orbital. The bonding and antibonding states between the present d_{xy/x^2-y^2} and $d_{xz/yz}$ orbitals correspond to the e'_g and e_g orbitals, respectively.